The study of $B \to K^{(*)}l^+l^-$ decays in family non-universal Z′ models*

Cheng-Wei Chiang(蒋正伟)[2,3] LI Run-Hui(李润辉)[1,4] LÜ Cai-Dian(吕才典)[1]

[1] Institute of High Energy Physics and Theoretical Physics Center for Science Facilities, Chinese Academy of Sciences, P.O. Box 918(4), Beijing 100049, China
[2] Department of Physics and Center for Mathematics and Theoretical Physics, National Central University, Chungli 320, China
[3] Institute of Physics, AS, Taipei 115, China
[4] School of Physics, Shandong University, Jinan 250100, China

Abstract: In a combined investigation of $B \to K^{(*)}l^+l^-$ decays, constraints on the related couplings in family non-universal Z′ models are derived. We find that within the allowed parameter space, the recently observed forward-backward asymmetry in the $B \to K^*l^+l^-$ decay can be explained by flipping the signs of the Wilson coefficients $C_9^{\rm eff}$ and C_{10}. With the obtained constraints, we also calculate the branching ratio of the $B_s \to \mu^+\mu^-$ decay. The upper bound of our prediction is nearly an order of magnitude smaller than the upper bound given by the CDF Collaboration recently.

Key words: forward-backward asymmetry, new physics, semi-leptonic decay

PACS: 13.25.Hw, 12.38.Bx **DOI:** 10.1088/1674-1137/36/1/003

1 Introduction

$B \to K^{(*)}l^+l^-$ decays play a very important role in heavy flavor physics. At the quark level, these decays involve the flavor-changing neutral current (FCNC) of the $b \to s$ transition, which is a purely quantum loop-mediated effect in the Standard Model (SM). These decay modes have therefore been proposed to test the SM predictions [1]. In addition to the branching ratio, several observables of the $B \to K^*l^+l^-$ decay, such as the longitudinal polarization fraction, the forward-backward asymmetry ($A_{\rm FB}$), the isospin symmetry and the transverse asymmetry, have been proposed to probe possible new physics (NP) [2]. Various NP models have thus been scrutinized for their effects on these observables [3].

A few years ago, the forward-backward asymmetry of $B \to K^*l^+l^-$ was first observed by the Belle Collaboration [4]. The BaBar Collaboration also published its results in this channel earlier this year [5, 6]. Recently, the Belle Collaboration updated its measurements in $B \to K^{(*)}l^+l^-$ decays [7]. In these experiments, forward-backward asymmetry is measured as a function of $q^2 = M_{ll}^2c^2$, the invariant mass of the lepton pair. In comparison, BaBar only has two q^2 bins of data, while Belle has six. Their fitted $A_{\rm FB}$ spectrum is generally higher than the SM expectation in all q^2 bins. This inspired us to do further investigations on these decays and see whether any NP models can better explain the experimental data.

In this paper, we consider a class of family non-universal Z′ models that induce FCNC's at tree level [8]. In such models, fermions in different families have different couplings to the Z′ boson in the gauge basis. After rotating to the physical basis, off-diagonal couplings are generally produced, inducing FCNC's at tree level. These FCNC couplings are subject to strong constraints from low-energy experiments. The phenomenological aspects of such models have been extensively analyzed by various groups in recent years [9–13]. In particular, the possible Z′-b-s coupling has received a lot of attention because it may explain some of the puzzling B physics data. Based on the

Received 14 April 2011, Revised 20 June 2011

* Supported by National Science Council of Taipei, (NSC 97-2112-M-008-002-MY3, NCTS), National Natural Science Foundation of China (10735080, 11075168, 10525523) and National Basic Research Program of China (973) (2010CB833000)

previous analysis, we study whether the recently observed B → K$^{(*)}$l$^+$l$^-$ data can be accommodated within this model as well.

This paper is organized as follows. In Section. 2 we first review the B → K$^{(*)}$l$^+$l$^-$ decays in the SM, and in the course of this we define the quantities relevant for the calculations, such as form factors, effective Hamiltonian, explicit formulas of the amplitudes, decays widths and forward-backward asymmetries. In Section 3 we describe the Z′ model with tree-level FCNC's and deduce its effects on the B → K$^{(*)}$l$^+$l$^-$ decays. We then use the observables to constrain the model parameters. We find that the observed data in B → K$^{(*)}$l$^+$l$^-$ can be accommodated in such a Z′ model. We also predict the range of $Br(\mathrm{B_s}\to\mu^+\mu^-)$ based on the constrained parameter space. Finally, we summarize our findings in Section 4.

2 B→K$^{(*)}$l$^+$l$^-$ decays in the standard model

2.1 Parametrization of the hadronic transitional matrix elements

The semileptonic decays investigated here involve hadronic matrix elements representing the B → K$^{(*)}$ transitions. Therefore, we first define the B → K form factors as follows:

$$\begin{aligned}\langle K(p)|\bar{s}\gamma_\mu b|B(p_{\rm B})\rangle &= f_+(q^2)\left\{(p_{\rm B}+p)_\mu-\frac{m_{\rm B}^2-m_{\rm K}^2}{q^2}q_\mu\right\}+\frac{m_{\rm B}^2-m_{\rm K}^2}{q^2}f_0(q^2)q_\mu\,,\\ \langle K(p)|\bar{s}\sigma_{\mu\nu}q^\nu b|B(p_{\rm B})\rangle &= {\rm i}(p_{\rm B}+p)_\mu q^2-q_\mu(m_{\rm B}^2-m_{\rm K}^2)\frac{f_{\rm T}(q^2)}{m_{\rm B}+m_{\rm K}}\,,\end{aligned}\tag{1}$$

where $q=p_{\rm B}-p$ is the momentum transfer to the lepton pairs. The B → K* transitional form factors are defined as:

$$\begin{aligned}\langle K^*(p,\epsilon^*)|\bar{q}\gamma^\mu b|\bar{B}(p_{\rm B})\rangle &= -\frac{2V(q^2)}{m_{\rm B}+m_{\rm K^*}}\epsilon^{\mu\nu\rho\sigma}\epsilon^*_\nu p_{{\rm B}\rho}p_\sigma,\\ \langle K^*(p,\epsilon^*)|\bar{q}\gamma^\mu\gamma_5 b|\bar{B}(p_{\rm B})\rangle &= 2{\rm i}m_{\rm K^*}A_0(q^2)\frac{\epsilon^*\cdot q}{q^2}q^\mu+{\rm i}(m_{\rm B}+m_{\rm K^*})A_1(q^2)\left[\epsilon^*_\mu-\frac{\epsilon^*\cdot q}{q^2}q^\mu\right]\\ &\quad -{\rm i}A_2(q^2)\frac{\epsilon^*\cdot q}{m_{\rm B}+m_{\rm K^*}}\left[(p_{\rm B}+p)^\mu-\frac{m_{\rm B}^2-m_{\rm K^*}^2}{q^2}q^\mu\right],\\ \langle K^*(p,\epsilon^*)|\bar{q}\sigma^{\mu\nu}q_\nu b|\bar{B}(p_{\rm B})\rangle &= -2{\rm i}T_1(q^2)\epsilon^{\mu\nu\rho\sigma}\epsilon^*_\nu p_{{\rm B}\rho}p_\sigma,\\ \langle K^*(p,\epsilon^*)|\bar{q}\sigma^{\mu\nu}\gamma_5 q_\nu b|\bar{B}(p_{\rm B})\rangle &= T_2(q^2)[(m_{\rm B}^2-m_{\rm K^*}^2)\epsilon^{*\mu}-(\epsilon^*\cdot q)(p_{\rm B}+p)^\mu]\\ &\quad +T_3(q^2)(\epsilon^*\cdot q)\left[q^\mu-\frac{q^2}{m_{\rm B}^2-m_{\rm K^*}^2}(p_{\rm B}+p)^\mu\right]\,.\end{aligned}\tag{2}$$

In the calculations of the semileptonic decays, we need the q^2 dependence in the form factors. For B → K* transitions, we adopt the dipole model parametrization for the form factors:

$$F(q^2)=\frac{F(0)}{1-a(q^2/m_{\rm B}^2)+b(q^2/m_{\rm B}^2)^2},\tag{3}$$

where a and b are parameters to be determined. We calculate the form factors in the PQCD approach [14] near the $q^2=0$ region, where the K* meson recoils very quickly, and determine their values at some points. Then we extrapolate our results to the entire kinematic regime through fitting. Our results in the PQCD approach, as well as those obtained using QCD sum rules (QCDSR) [15], are listed in Table 1. In our calculations we mainly use the PQCD results. The QCDSR results are included only as a comparison because we do not have the explicit errors on the QCDSR results.

For the form factors of the B → K transition, we adopt a different parametrization:

$$\begin{aligned}F(q^2) &= F(0)\exp[c_1(q^2/m_{\rm B}^2)+c_2(q^2/m_{\rm B}^2)^2\\ &\quad +c_3(q^2/m_{\rm B}^2)^3],\end{aligned}\tag{4}$$

because the authors of Ref. [16] find that in their fitting, the extrapolation of the dipole parametrization to maximum q^2 is prone to reach a serious singularity below the physical cut starting at $q^2=m_{\rm B}^2$. The values of the parameters in the B → K form factors [16] are listed in Table 2.

Table 1. $B \to K^*$ form factors in the PQCD approach and QCD sum rules (QCDSR).

	PQCD	QCDSR [15]		PQCD	QCDSR [15]
$V(0)$	0.26	0.458	$T_1(0)$	0.23	0.379
$a(V)$	1.75	1.55	$a(T_1)$	1.70	1.59
$b(V)$	0.68	0.575	$b(T_1)$	0.63	0.615
$A_0(0)$	0.30	0.470	$T_2(0)$	0.23	0.379
$a(A_0)$	1.72	1.55	$a(T_2)$	0.71	0.49
$b(A_0)$	0.62	0.680	$b(T_2)$	−0.19	−0.241
$A_1(0)$	0.19	0.337	$T_3(0)$	0.20	0.261
$a(A_1)$	0.79	0.60	$a(T_3)$	1.58	1.20
$b(A_1)$	−0.09	−0.023	$b(T_3)$	0.49	0.098
$A_2(0)$		0.283			
$a(A_2)$		1.18			
$b(A_2)$		0.281			

Table 2. $B \to K$ form factors in the light cone sum rules with parametrization, Eq. (4).

	$F(0)$	c_1	c_2	c_3
$f_+(q^2)$	0.319	1.465	0.372	0.782
$f_0(q^2)$	0.319	0.633	−0.095	0.591
$f_T(q^2)$	0.355	1.478	0.373	0.700

2.2 Effective Hamiltonian and decay amplitudes

At the quark level, the $B \to K^{(*)}l^+l^-$ decays are dominated by the $b \to sl^+l^-$ transition, the Hamiltonian for which is given by

$$\mathcal{H}_{\rm eff} = -\frac{G_{\rm F}}{\sqrt{2}} V_{\rm tb}V_{\rm ts}^* \sum_{i=1}^{10} C_i(\mu) O_i(\mu), \tag{5}$$

where $V_{\rm tb}$ and $V_{\rm ts}$ are the Cabibbo-Kobayashi-Maskawa matrix elements and $C_i(\mu)$ is the Wilson coefficient evaluated at the scale μ. The local operators $O_i(\mu)$ are given by [17]

$$\begin{aligned}
O_1 &= (\bar{s}_\alpha c_\alpha)_{V-A}(\bar{c}_\beta b_\beta)_{V-A},\\
O_2 &= (\bar{s}_\alpha c_\beta)_{V-A}(\bar{c}_\beta b_\alpha)_{V-A},\\
O_3 &= (\bar{s}_\alpha b_\alpha)_{V-A}\sum_q (\bar{q}_\beta q_\beta)_{V-A},\\
O_4 &= (\bar{s}_\alpha b_\beta)_{V-A}\sum_q (\bar{q}_\beta q_\alpha)_{V-A},\\
O_5 &= (\bar{s}_\alpha b_\alpha)_{V-A}\sum_q (\bar{q}_\beta q_\beta)_{V+A},\\
O_6 &= (\bar{s}_\alpha b_\beta)_{V-A}\sum_q (\bar{q}_\beta q_\alpha)_{V+A},\\
O_7 &= \frac{em_b}{8\pi^2}\bar{s}\sigma^{\mu\nu}(1+\gamma_5)bF_{\mu\nu} + \frac{em_s}{8\pi^2}\bar{s}\sigma^{\mu\nu}(1-\gamma_5)bF_{\mu\nu},\\
O_9 &= \frac{\alpha_{\rm em}}{2\pi}(\bar{\ell}\gamma_\mu\ell)(\bar{s}\gamma^\mu(1-\gamma_5)b),\\
O_{10} &= \frac{\alpha_{\rm em}}{2\pi}(\bar{\ell}\gamma_\mu\gamma_5\ell)(\bar{s}\gamma^\mu(1-\gamma_5)b)\ ,
\end{aligned} \tag{6}$$

where α and β are color indices, q=u, d, s, c, $(\bar{q}_1q_2)_{V-A}(\bar{q}_3q_4)_{V-A} \equiv [\bar{q}_1\gamma^\mu(1-\gamma_5)q_2][\bar{q}_3\gamma_\mu(1-\gamma_5)q_4]$, and $(\bar{q}_1q_2)_{V-A}(\bar{q}_3q_4)_{V+A} \equiv [\bar{q}_1\gamma^\mu(1-\gamma_5)q_2][\bar{q}_3\gamma_\mu(1+\gamma_5)q_4]$.

With the above Hamiltonian, the amplitude of the $b \to sl^+l^-$ transition can be written as

$$\begin{aligned}
&\mathcal{A}(b \to sl^+l^-)\\
&= \frac{G_{\rm F}}{2\sqrt{2}}\frac{\alpha_{\rm em}}{\pi}V_{\rm tb}V_{\rm ts}^*\Bigg\{C_9^{\rm eff}(q^2)[\bar{s}\gamma_\mu(1-\gamma_5)b][\bar{\ell}\gamma^\mu\ell]\\
&+C_{10}[\bar{s}\gamma_\mu(1-\gamma_5)b][\bar{\ell}\gamma^\mu\gamma_5\ell]\\
&-2m_bC_7^{\rm eff}\left[\bar{s}i\sigma_{\mu\nu}\frac{q^\nu}{q^2}(1+\gamma_5)b\right][\bar{\ell}\gamma^\mu\ell]\\
&-2m_sC_7^{\rm eff}\left[\bar{s}i\sigma_{\mu\nu}\frac{q^\nu}{q^2}(1-\gamma_5)b\right][\bar{\ell}\gamma^\mu\ell]\Bigg\},
\end{aligned} \tag{7}$$

where m_b is the b quark mass in the $\overline{\rm MS}$ scheme. The Wilson coefficients $C_7^{\rm eff} = C_7 - C_5/3 - C_6$ and $C_9^{\rm eff}$ contain both the long-distance and short-distance contributions:

$$C_9^{\rm eff}(q^2) = C_9(\mu) + Y_{\rm pert}(q^2) + Y_{\rm LD}(q^2). \tag{8}$$

Here $Y_{\rm pert}$ represents the perturbative contribution, and $Y_{\rm LD}$ is the long-distance part containing contributions from the resonant states and can be excluded by experimental analysis. Thus we will not include $Y_{\rm LD}$ in our calculation, and

$$C_9^{\rm eff}(q^2) = C_9(\mu) + Y_{\rm pert}(q^2), \tag{9}$$

with the detailed form of $Y_{\rm pert}$ given in Ref. [18]. The values of the wilson coefficients in SM are listed in Table 3.

Table 3. Values of Wilson coefficients $C_i(m_{\rm b})$ in the leading logarithmic approximation, with $m_{\rm W}=80.4$ GeV, $\mu=m_{\rm b,pole}$ [17].

C_1	C_2	C_3	C_4	C_5	C_6	$C_7^{\rm eff}$	C_9	C_{10}
1.107	−0.248	−0.011	−0.026	−0.007	−0.031	−0.313	4.344	−4.669

The B → K*l$^+$l$^-$ decay is more complicated because of its polarization structures in the final state. We will use the helicity basis. By re-expressing the metric tensor

$$g_{\mu\nu}=-\sum_{\lambda}\epsilon_{\mu}(\lambda)\epsilon^{*}_{\nu}(\lambda)+\frac{q_{\mu}q_{\nu}}{q^2}, \tag{10}$$

we can decompose the amplitude $\mathcal{A}(\bar{\rm B}\to{\rm K}^*{\rm l}^+{\rm l}^-)$ into the Lorentz-invariant leptonic part $L(L/R,\lambda)$ and the hadronic part $H(L/R,\lambda)$:

$$\begin{aligned}\mathcal{A}(\bar{\rm B}\to\bar{\rm K}^*{\rm l}^+{\rm l}^-)=&\ L_{\mu}(L)H_{\nu}(L)g^{\mu\nu}+L_{\mu}(R)H_{\nu}(R)g^{\mu\nu}\\ =&\ -\sum_{\lambda}L(L,\lambda)H(L,\lambda)\\ &-\sum_{\lambda}L(R,\lambda)H(R,\lambda).\end{aligned} \tag{11}$$

The details have been given in Appendix C of Ref. [19]. The explicit formulas of the functions $L(L/R,\lambda)$ and $H(L/R,\lambda)$ are listed in Appendix A.

2.3 The decay widths and branching ratios

With the form factors given in Section 2.1 and Eq. (7), we obtain the dilepton spectrum of B → Kl$^+$l$^-$ as

$$\begin{aligned}&\frac{{\rm d}\Gamma_i({\rm B}\to{\rm Kl}^+{\rm l}^-)}{{\rm d}q^2}\\ =&\ \frac{G_{\rm F}^2|V_{\rm tb}|^2|V_{\rm ts}^*|^2\alpha_{\rm em}^2\lambda^{3/2}}{1536\pi^5 m_{\rm B}^3}\Bigg\{|C_{10}f_+(q^2)|^2\\ &+\left|C_9^{\rm eff}f_+(q^2)+\frac{2C_7^{\rm eff}(m_{\rm b}+m_{\rm s})}{m_{\rm B}+m_{\rm K}}f_{\rm T}(q^2)\right|^2\Bigg\},\end{aligned} \tag{12}$$

where

$$\begin{aligned}\lambda=&\ (m_{\rm K^*}^2+m_{\rm B}^2-q^2)^2-4m_{\rm B}^2m_{\rm K^*}^2\\ =&\ (m_{\rm B}^2-m_{\rm K^*}^2-q^2)^2-4m_{\rm K^*}^2q^2.\end{aligned} \tag{13}$$

For the B → K*l$^+$l$^-$ decay, we define the direction opposite to the momentum of the K* meson in the rest frame of the B meson as the $+z$ direction. In the center-of-mass frame of l$^+$l$^-$, θ_1 is defined as the angle between the z axis and the momentum of l$^-$. In the experiment, the K* meson usually decays to the Kπ final state. We define the angle between the decay plane K* → Kπ and the plane determined by l$^+$l$^-$ as ϕ. Combining the leptonic amplitudes, the hadronic amplitudes and the phase space, the partial decay width of B → K*l$^+$l$^-$ is given by

$$\begin{aligned}&{\rm d}\Gamma_i(\bar{\rm B}\to\bar{\rm K}^*{\rm l}^+{\rm l}^-)\\ =&\ \frac{\sqrt{\lambda}}{1024\pi^4 m_{\rm B}^3}{\rm d}\cos\theta_1{\rm d}\phi{\rm d}q^2|\mathcal{A}_i({\rm B}\to{\rm K}^*{\rm l}^+{\rm l}^-)|^2\\ =&\ \frac{\sqrt{\lambda}}{1024\pi^4 m_{\rm B}^3}{\rm d}\cos\theta_1{\rm d}\phi{\rm d}q^2(|L(L,i)H(L,i)|^2\\ &+|L(R,i)H(R,i)|^2)\ ,\end{aligned} \tag{14}$$

where $i=0,+$ or $-$ denotes the three different polarizations of the K*.

After integrating out θ_1 and ϕ in Eq. (14), one obtains the dilepton spectrum of the B → K*l$^+$l$^-$ decay as:

$$\begin{aligned}&\frac{{\rm d}\Gamma_i({\rm B}\to{\rm K}^*{\rm l}^+{\rm l}^-)}{{\rm d}q^2}\\ =&\ \frac{\sqrt{\lambda}q^2}{96\pi^3 m_{\rm B}^3}\left[|H(L,i)|^2+|H(R,i)|^2\right].\end{aligned} \tag{15}$$

In Section 2.2, one can find that among the Wilson coefficients only $C_9^{\rm eff}$ has the q^2 dependence. The dilepton spectra of B → K$^{(*)}$l$^+$l$^-$ decays are shown in Fig. 1, with and without $Y_{\rm pert}(q^2)$ in $C_9^{\rm eff}$ included. After further integrating out the q^2 dependence, we obtain the total branching ratios:

$$Br({\rm B}\to{\rm Kl}^+{\rm l}^-)=\begin{cases}(4.70^{+1.29}_{-0.71})\times10^{-7}\,(q^2\text{ part in }C_9^{\rm eff}\text{ included}),\\ (4.45^{+1.22}_{-0.67})\times10^{-7}\,(q^2\text{ part in }C_9^{\rm eff}\text{ excluded}),\end{cases} \tag{16}$$

$$Br({\rm B}\to{\rm K}^*{\rm l}^+{\rm l}^-)=\begin{cases}(16.5^{+7.8}_{-5.7})\times10^{-7}\,(q^2\text{ part in }C_9^{\rm eff}\text{ included}),\\ (15.8^{+7.5}_{-5.5})\times10^{-7}\,(q^2\text{ part in }C_9^{\rm eff}\text{ excluded}).\end{cases} \tag{17}$$

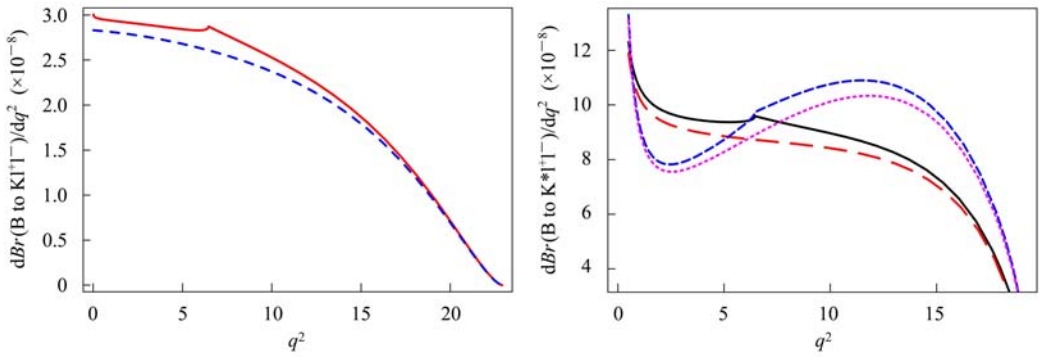

Fig. 1. q^2-dependence of the branching ratios of the $B \to Kl^+l^-$ (left plot) and $B \to K^*l^+l^-$ (right plot) decays. In the left plot, the red solid (blue dashed) curve stands for the dilepton spectrum with (without) the $Y_{\rm pert}(q^2)$ part included in $C_9^{\rm eff}$. The right plot shows the spectrum predicted in PQCD and QCDSR with and without the $Y_{\rm pert}(q^2)$ part in Eq. (9). The black solid (red long dashed) curve is the PQCD result with (without) $Y_{\rm pert}(q^2)$ and the blue short dashed (pink dotted) curve is the QCDSR result with (without) $Y_{\rm pert}(q^2)$. In the curves where $Y_{\rm pert}(q^2)$ is included, a kink shows up because it is a piecewise function.

These predictions are to be compared with the experimental results [7]:

$$\begin{aligned} Br(B\to Kl^+l^-) &= (4.8^{+0.5}_{-0.4}\pm 0.3)\times 10^{-7},\\ Br(B\to K^*l^+l^-) &= (10.7^{+1.1}_{-1.0}\pm 0.9)\times 10^{-7}. \end{aligned} \tag{18}$$

From Fig. 1, Eq. (16) and Eq. (17), one finds that the $Y_{\rm pert}(q^2)$ piece in $C_9^{\rm eff}$ has a small effect on the branching ratios in comparison with other uncertainties. To simplify the notation, we define $C_9' \equiv Y_{\rm pert}(q^2)$, and thus $C_9^{\rm eff} = C_9 + C_9'$. The differential branching ratio of $B \to Kl^+l^-$ is then decomposed into the following form

$$\begin{aligned} &\frac{{\rm d}Br(B\to Kl^+l^-)}{{\rm d}q^2}\\ &= |C_{10}|^2B_1' + |C_9^{\rm eff}|^2B_2' + |C_7^{\rm eff}|^2B_3' + 2{\rm Re}[C_9^{\rm eff}C_7^{\rm eff*}]B_4'\\ &= |C_{10}|^2B_1' + [|C_9|^2 + |C_9'|^2 + 2{\rm Re}[C_9C_9'^*]]B_2'\\ &\quad + |C_7^{\rm eff}|^2B_3' + 2{\rm Re}[(C_9+C_9')C_7^{\rm eff*}]B_4'. \end{aligned} \tag{19}$$

After the integration over q^2, Eq. (19) can be rearranged as

$$\begin{aligned} Br(B\to Kl^+l^-) &= |C_{10}|^2B_1 + |C_9|^2B_2 + |C_7^{\rm eff}|^2B_3\\ &\quad + 2{\rm Re}[C_9C_7^{\rm eff*}]B_4 + 2{\rm Re}[C_9]B_5\\ &\quad + 2{\rm Re}[C_7^{\rm eff}]B_6 + B_7, \end{aligned} \tag{20}$$

where B_5 (B_6, B_7) contains the integration of ${\rm Re}[C_9']$ B_2' (${\rm Re}[C_9']B_4'$, $|C_9'|^2B_2'$). Similarly, $Br(B \to K^*l^+l^-)$ is decomposed as

$$\begin{aligned} Br(B\to K^*l^+l^-) &= |C_{10}|^2B_1^* + |C_9|^2B_2^* + |C_7^{\rm eff}|^2B_3^*\\ &\quad + 2{\rm Re}[C_9C_7^{\rm eff*}]B_4^* + 2{\rm Re}[C_9]B_5^*\\ &\quad + 2{\rm Re}[C_7^{\rm eff}]B_6^* + B_7^*. \end{aligned} \tag{21}$$

The values of $B_j^{(*)}$ with $j = 1,2,3,...,7$ are, in units of 10^{-8} (10^{-7}),

$$\begin{aligned} B_1 &= 1.28^{+0.30}_{-0.23},\ B_2 = B_1,\ B_3 = 4.41^{+1.44}_{-0.82},\\ B_4 &= 2.33^{+0.71}_{-0.39},\ B_5 = 0.31^{+0.09}_{-0.05},\ B_6 = 0.58^{+0.19}_{-0.10},\\ B_7 &= 0.18^{+0.04}_{-0.03},\ B_1^* = 0.41^{+0.20}_{-0.15},\ B_2^* = B_1^*,\\ B_3^* &= 12.74^{+6.35}_{-4.86},\ B_4^* = 0.84^{+0.46}_{-0.45},\ B_5^* = 0.09^{+0.04}_{-0.03},\\ B_6^* &= 0.18^{+0.10}_{-0.10},\ B_7^* = 0.04^{+0.02}_{-0.02}. \end{aligned} \tag{22}$$

These values will be used to constrain the couplings in the Z′ model later. From Fig. 1 and Eqs. (A7) to (A12), one can find a pole at $q^2 = 0$ in ${\rm d}Br(B \to K^*l^+l^-)/{\rm d}q^2$. That is why B_3^* is much larger than the others.

2.4 The forward-backward asymmetry

The differential forward-backward asymmetry of $\bar{B} \to \bar{K}^*l^+l^-$ is defined by

$$\frac{{\rm d}A_{\rm FB}}{{\rm d}q^2} = \int_0^1 {\rm d}\cos\theta_l \frac{{\rm d}^2\Gamma}{{\rm d}q^2{\rm d}\cos\theta_l} - \int_{-1}^0 {\rm d}\cos\theta_l \frac{{\rm d}^2\Gamma}{{\rm d}q^2{\rm d}\cos\theta_l}, \tag{23}$$

while the normalized differential forward-backward asymmetry is defined by

$$\frac{{\rm d}\bar{A}_{\rm FB}}{{\rm d}q^2} = \frac{\frac{{\rm d}A_{\rm FB}}{{\rm d}q^2}}{\frac{{\rm d}\Gamma}{{\rm d}q^2}} = \frac{3}{4}\frac{-|H(L,+)|^2 + |H(R,+)|^2 + |H(L,-)|^2 - |H(R,-)|^2}{|H(L,0)|^2 + |H(R,0)|^2 + |H(L,+)|^2 + |H(R,+)|^2 + |H(L,-)|^2 + |H(R,-)|^2}. \tag{24}$$

Substituting the expressions in Eqs. (A7) to (A12) into Eq. (24), we get the explicit expression for $\frac{\mathrm{d}\bar{A}_{\mathrm{FB}}}{\mathrm{d}q^2}$ as follows:

$$\frac{\mathrm{d}\bar{A}_{\mathrm{FB}}}{\mathrm{d}q^2}=\frac{3N(q^2)}{4D(q^2)}, \tag{25}$$

where

$$\begin{aligned}
N(q^2) &= |V_{\mathrm{tb}}|^2|V_{\mathrm{ts}}^*|^2G_{\mathrm{F}}^2\alpha_{\mathrm{em}}^2\sqrt{\lambda}q^2\{-\mathrm{Re}[C_{10}]C_7^{\mathrm{eff}}m_{\mathrm{b}}\\
&\quad\times[(m_{\mathrm{B}}+m_{\mathrm{K}^*})A_1(q^2)T_1(q^2)\\
&\quad+(m_{\mathrm{B}}-m_{\mathrm{K}^*})T_2(q^2)V(q^2)]\\
&\quad+\mathrm{Re}[C_9^{\mathrm{eff}}C_{10}^*][-q^2V(q^2)A_1(q^2)]\},\\
D(q^2) &= 2\pi^2(q^2)^2[|H(L,0)|^2+|H(R,0)|^2\\
&\quad+|H(L,+)|^2+|H(R,+)|^2\\
&\quad+|H(L,-)|^2+|H(R,-)|^2].
\end{aligned} \tag{26}$$

In the above expression, terms suppressed by m_{s} are dropped for simplicity. As can be explicitly checked, the pole in the dilepton spectrum at $q^2=0$ disappears in the denominator.

According to Eq. (26), the numerator of $\mathrm{d}A_{\mathrm{FB}}/\mathrm{d}q^2$ is zero at $q^2=0$ because of the common factor q^2, while the denominator has a non-zero value because its common factor $(q^2)^2$ cancels with the $(q^2)^2$ factor arising from Eqs. (A8), (A9), (A11) and (A12). Thus $\mathrm{d}A_{\mathrm{FB}}/\mathrm{d}q^2=0$ at $q^2=0$. In the SM, $C_7^{\mathrm{eff}}<0$, $C_9^{\mathrm{eff}}>0$ and $C_{10}<0$; thus the first term in the curly bracket of $N(q^2)$ is negative and the second term is positive. In the regime where q^2 is near zero, the first term gives the dominant contribution since the second term is suppressed by the small q^2. Therefore, the sign of $\mathrm{d}A_{\mathrm{FB}}/\mathrm{d}q^2$ is determined by the first term and gives a negative value. As q^2 increases, the second term becomes dominant. There exists a point where $\mathrm{d}A_{\mathrm{FB}}/\mathrm{d}q^2$ becomes zero: the so-called forward-backward asymmetry zero. The position of the zero is determined by C_7^{eff} and C_9^{eff}, as the form-factor dependence drops at the leading order [2]. As q^2 becomes even larger, the effect of the overall factor $\sqrt{\lambda}$ becomes crucial. Eq. (13) tells us that $\lambda=0$ at the largest recoil where $q^2=(m_{\mathrm{B}}-m_{\mathrm{K}^*})^2$. Therefore, $\mathrm{d}A_{\mathrm{FB}}/\mathrm{d}q^2$ falls back to zero at the end of the kinematic regime. All these behaviors of $\mathrm{d}A_{\mathrm{FB}}/\mathrm{d}q^2$ can be observed in Fig. 2. The red dashed curve is drawn with the contribution of only the second term in the curly bracket of $N(q^2)$. This shows the importance of C_7^{eff} in the low q^2 regime.

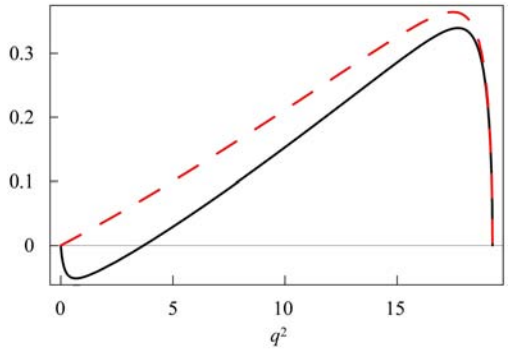

Fig. 2. The forward-backward asymmetry for B → K*l$^+$l$^-$, with form factors given by the PQCD approach. The black solid curve is given with SM C_7 and the red dashed curve is given with $C_7=0$.

However, the latest Belle data [7] do not show an obvious zero for $\mathrm{d}A_{\mathrm{FB}}/\mathrm{d}q^2$, and the values at all q^2 are consistently higher than the SM expectation. A common solution is to flip the sign of C_7^{eff} as it is still consistent with the constraint from B → X$_{\mathrm{s}}\gamma$ data. In the next section, we offer an alternative solution in the family non-universal Z′ model.

3 Constraints on the couplings in Z′ physics

3.1 b → sl$^+$l$^-$ in the Z′ FCNC model

In the appropriate gauge basis, the $U(1)'$ currents are

$$J_{\mathrm{Z}'}^{\mu}=g'\sum_i\bar{\psi}_i\gamma^{\mu}[\epsilon_i^{\psi_{\mathrm{L}}}P_{\mathrm{L}}+\epsilon_i^{\psi_{\mathrm{R}}}P_{\mathrm{R}}]\psi_i, \tag{27}$$

where i is the family index and ψ labels the fermions (up- or down-type quarks, or charged or neutral leptons), and $P_{\mathrm{L,R}}=(1\mp\gamma_5)/2$. According to some string construction or GUT models such as E_6, it is possible to have family non-universal Z′ couplings. That is, even though $\epsilon_i^{\mathrm{L,R}}$ are diagonal, the couplings are not family universal. After rotating to the physical basis, FCNCs generally appear at tree level in both the left-handed (LH) and right-handed (RH) sectors. Explicitly,

$$B^{\psi_{\mathrm{L}}}=V_{\psi_{\mathrm{L}}}\epsilon^{\psi_{\mathrm{L}}}V_{\psi_{\mathrm{L}}}^{\dagger},\quad B^{\psi_{\mathrm{R}}}=V_{\psi_{\mathrm{R}}}\epsilon^{\psi_{\mathrm{R}}}V_{\psi_{\mathrm{R}}}^{\dagger}. \tag{28}$$

Moreover, these couplings may contain CP-violating phases beyond that of the SM.

In particular, Z′$\bar{\mathrm{b}}$s couplings can be generated:

$$\mathcal{L}_{\mathrm{FCNC}}^{\mathrm{Z}'}=-g'(B_{\mathrm{sb}}^{\mathrm{L}}\bar{s}_{\mathrm{L}}\gamma_{\mu}b_{\mathrm{L}}+B_{\mathrm{sb}}^{\mathrm{R}}\bar{s}_{\mathrm{R}}\gamma_{\mu}b_{\mathrm{R}})Z'^{\mu}+\mathrm{h.c.}. \tag{29}$$

The couplings in Eq. (29) lead to extra contributions to the b → sl$^+$l$^-$ decay at tree level, mediated by a

virtual Z′ boson. The amplitude is given by

$$\frac{g'^2}{M_{Z'}^2}\left(B_{\rm sb}^{\rm L}\bar{s}_{\rm L}\gamma_\mu b_{\rm L}+B_{\rm sb}^{\rm R}\bar{s}_{\rm R}\gamma_\mu b_{\rm R}\right)\left(B_{\rm ll}^{\rm L}\bar{\ell}_{\rm L}\gamma^\mu l_{\rm L}\right.$$

$$\left.+B_{\rm ll}^{\rm R}\bar{\ell}_{\rm R}\gamma^\mu\ell_{\rm R}\right). \quad (30)$$

There are thus four types of operators, $O_{\rm LL}$, $O_{\rm LR}$, $O_{\rm RL}$ and $O_{\rm RR}$. The above amplitude can be derived from an effective Hamiltonian

$$\mathcal{H}_{\rm eff}^{\rm Z'} = \frac{8G_{\rm F}}{\sqrt{2}}(\rho_{\rm sb}^{\rm L}\bar{s}_{\rm L}\gamma_\mu b_{\rm L}+\rho_{\rm sb}^{\rm R}\bar{s}_{\rm R}\gamma_\mu b_{\rm R})(\rho_{\rm ll}^{\rm L}\bar{\ell}_{\rm L}\gamma^\mu\ell_{\rm L}$$

$$+\rho_{\rm ll}^{\rm R}\bar{\ell}_{\rm R}\gamma^\mu\ell_{\rm R}), \quad (31)$$

where

$$\rho_{\rm ff'}^{\rm L,R}\equiv\frac{g'M_{\rm Z}}{gM_{\rm Z'}}B_{\rm ff'}^{\rm L,R}, \quad (32)$$

and g is the coupling associated with the $SU(2)_{\rm L}$ group in the SM. Throughout this analysis, we ignore the renormalization group running effects due to these new contributions because they are expected to be small.

3.2 Constraints from the B→K$^{(*)}$l$^+$l$^-$ decays

For the purpose of illustration and to avoid too many free parameters, we assume that the FCNC couplings of the Z′ and quarks only occur in the LH sector. Therefore, $\rho_{\rm sb}^{\rm R}=0$ and the effects of the Z′ FCNC currents simply modify the Wilson coefficients C_9 and C_{10} in Eq. (5). We denote these two modified Wilson coefficients by $C_9^{\rm eff,Z'}$ and $C_{10}^{\rm Z'}$, respectively. More explicitly,

$$\begin{aligned}
{\rm Re}[C_9^{\rm eff,Z'}] &= {\rm Re}[C_9^{\rm eff}]-\frac{4\pi{\rm Re}[\rho_{\rm sb}^{\rm L}](\rho_{\rm ll}^{\rm L}+\rho_{\rm ll}^{\rm R})}{V_{\rm tb}V_{\rm ts}^*\alpha_{\rm em}},\\
{\rm Im}[C_9^{\rm eff,Z'}] &= {\rm Im}[C_9^{\rm eff}]-\frac{4\pi{\rm Im}[\rho_{\rm sb}^{\rm L}](\rho_{\rm ll}^{\rm L}+\rho_{\rm ll}^{\rm R})}{V_{\rm tb}V_{\rm ts}^*\alpha_{\rm em}},\\
{\rm Re}[C_{10}^{\rm Z'}] &= C_{10}-\frac{4\pi{\rm Re}[\rho_{\rm sb}^{\rm L}](\rho_{\rm ll}^{\rm R}-\rho_{\rm ll}^{\rm L})}{V_{\rm tb}V_{\rm ts}^*\alpha_{\rm em}},\\
{\rm Im}[C_{10}^{\rm Z'}] &= -\frac{4\pi{\rm Im}[\rho_{\rm sb}^{\rm L}](\rho_{\rm ll}^{\rm R}-\rho_{\rm ll}^{\rm L})}{V_{\rm tb}V_{\rm ts}^*\alpha_{\rm em}}.
\end{aligned} \quad (33)$$

For simplicity, we further assume that $\rho_{\rm sb}^{\rm L}$ is real. Then the imaginary part of $C_9^{\rm eff}$ will not be affected by the Z′ model, and $C_{10}^{\rm Z'}$ is still a real number.

First, we consider the constraint from the spectrum of ${\rm d}\bar{A}_{\rm FB}/{\rm d}q^2$. In order to fit the experimental data, a sign flip is needed for ${\rm d}\bar{A}_{\rm FB}/{\rm d}q^2$ near the $q^2=0$ regime. People usually consider the flipped-sign solution with $C_7=-C_7^{\rm SM}$, because it is still allowed by the B→X$_{\rm s}\gamma$ data. However, an alternative solution is to flip the signs of $C_9^{\rm eff}$ and C_{10} instead, as is possible in our model. Below Eq. (26), it is noted that in this regime the term proportional to ${\rm Re}[C_{10}]C_7^{\rm eff}$ dominates. Therefore, one can flip the sign of C_{10}:

$${\rm Re}[C_{10}^{\rm Z'}]>0. \quad (34)$$

Moreover, in order to keep the second term in the curly bracket of $N(q^2)$ with the correct behavior, we also need to flip the sign of ${\rm Re}[C_9^{\rm eff}]$. Thus, we require

$${\rm Re}[C_9^{\rm eff,Z'}]<0. \quad (35)$$

Eqs. (34) and (35) are the constraints from the ${\rm d}\bar{A}_{\rm FB}/{\rm d}q^2$ spectrum obtained by the Belle Collaboration (see Fig. 1 in Ref. [7]).

Next, we consider the constraints from the branching ratios of the B→K$^{(*)}$l$^+$l$^-$ decays. These constraints are obtained in the following way. After including the contributions of Z′, the upper (lower) bound of the theoretical predictions should be greater (smaller) than the experimental lower (upper) bound at the 2σ level. When we deal with the experimental data, we add the statistical and systematic errors in quadrature. With Eqs. (21) and (22), we have the following branching-ratio constraints:

$$B_{\rm 1u}^{(*)}(|C_{10}^{\rm Z'}|^2+|C_9^{\rm Z'}|^2)+B_{\rm 3u}^{(*)}|C_7^{\rm eff}|^2+B_{\rm 4u}^{(*)}{\rm Re}[C_9^{\rm Z'}C_7^{\rm eff*}]$$

$$+B_{\rm 5u}^{(*)}{\rm Re}[C_9^{\rm Z'}]+B_{\rm 6u}^{(*)}{\rm Re}[C_7^{\rm eff}]+B_{\rm 7u}^{(*)}>Br_{\rm exp}^{(*)}-2\sigma_{\rm l}^{(*)}, \quad (36)$$

$$B_{\rm 1l}^{(*)}(|C_{10}^{\rm Z'}|^2+|C_9^{\rm Z'}|^2)+B_{\rm 3l}^{(*)}|C_7^{\rm eff}|^2+B_{\rm 4l}^{(*)}{\rm Re}[C_9^{\rm Z'}C_7^{\rm eff*}]$$

$$+B_{\rm 5l}^{(*)}{\rm Re}[C_9^{\rm Z'}]+B_{\rm 6l}^{(*)}{\rm Re}[C_7^{\rm eff}]+B_{\rm 7l}^{(*)}<Br_{\rm exp}^{(*)}+2\sigma_{\rm u}^{(*)}, \quad (37)$$

where quantities with a star in the superscript are for the B→K*l$^+$l$^-$ decay, the letters "u" and "l" in the subscript represent the 1-σ upper and lower bounds of the corresponding quantity $B_i^{(*)}$, respectively, and $Br_{\rm exp}^{(*)}$ denote the central values of the B→K$^{(*)}$l$^+$l$^-$ branching ratios.

Moreover, $C_9^{\rm Z'}=C_9+x$ with $Y_{\rm pert}(q^2)$ excluded, and $C_{10}^{\rm Z'}=C_{10}+y$, where

$$x = -\frac{4\pi{\rm Re}[\rho_{\rm sb}^{\rm L}](\rho_{\rm ll}^{\rm L}+\rho_{\rm ll}^{\rm R})}{V_{\rm tb}V_{\rm ts}^*\alpha_{\rm em}}, \quad (38)$$

$$y = -\frac{4\pi{\rm Re}[\rho_{\rm sb}^{\rm L}](\rho_{\rm ll}^{\rm R}-\rho_{\rm ll}^{\rm L})}{V_{\rm tb}V_{\rm ts}^*\alpha_{\rm em}}. \quad (39)$$

Then Eqs. (36) and (37) can be rearranged as

$$B_{1u}^{(*)}(x+T_u^{(*)})^2+B_{1u}^{(*)}(y+C_{10})^2 +C_u^{(*)}>Br_{exp}^{(*)}-2\sigma_l^{(*)}, \quad (40)$$

$$B_{1l}^{(*)}(x+T_l^{(*)})^2+B_{1l}^{(*)}(y+C_{10})^2 +C_l^{(*)}<Br_{exp}^{(*)}+2\sigma_u^{(*)}, \quad (41)$$

where

$$T_{u/l}^{(*)} = \frac{2B_{1u/l}^{(*)}C_9+B_{4u/l}^{(*)}C_7^{eff}+B_{5u/l}^{(*)}}{2B_{1u/l}^{(*)}},$$

$$C_{u/l}^{(*)} = B_{1u/l}^{(*)}C_9^2+B_{7u/l}^{(*)}(C_7^{eff})^2+B_{4u/l}^{(*)}C_7^{eff}C_9 +B_{5u/l}^{(*)}C_9+B_{6u/l}^{(*)}C_7+B_{7u/l}^{(*)} -B_{1u/l}^{(*)}\left(T_{u/l}^{(*)}\right)^2. \quad (42)$$

Substituting all the numerical values in Eqs. (34), (35), (40) and (41), we have

$$x<-4.344, \quad (43)$$

$$y>4.669, \quad (44)$$

$$1.58(x+3.99)^2+1.58(y-4.669)^2-37.88>0, \quad (45)$$

$$1.05(x+4.01)^2+1.05(y-4.669)^2-59.58<0, \quad (46)$$

$$0.61(x+3.89)^2+0.61(y-4.669)^2-6.38>0, \quad (47)$$

$$0.26(x+4.11)^2+0.26(y-4.669)^2-12.81<0. \quad (48)$$

Eqs. (43)–(48) give the constraints on x and y, which are shown in Fig. 3. The common area of the above six conditions is outside the red solid circle and inside the blue long dashed circle, to the left of the solid vertical line $x=-C_9$ and above the solid horizontal line $y=-C_{10}$. This area gives

$$-\sqrt{(Br_{exp}^*+2\sigma_u^*-C_l^*)/B_{1l}^*}-T_l^*\lesssim x\lesssim -C_9, \quad -C_{10}\lesssim y\lesssim\sqrt{(Br_{exp}^*+2\sigma_u^*-C_l^*)/B_{1l}^*}-C_{10}. \quad (49)$$

With Eqs. (38) and (39), we have

$$\left[\sqrt{(Br_{exp}^*+2\sigma_u^*-C_l^*)/B_{1l}^*}-C_{10}-C_9\right]\mathcal{K}\lesssim \mathrm{Re}[\rho_{sb}^L]\rho_{ll}^R \lesssim\left[-\sqrt{(Br_{exp}^*+2\sigma_u^*-C_l^*)/B_{1l}^*}-T_l^*-C_{10}\right]\mathcal{K},$$

$$[C_{10}-C_9]\mathcal{K}\lesssim \mathrm{Re}[\rho_{sb}^L]\rho_{ll}^L \lesssim\left[-2\sqrt{(Br_{exp}^*+2\sigma_u^*-C_l^*)/B_{1l}^*}-T_l^*+C_{10}\right]\mathcal{K}, \quad (50)$$

with $\mathcal{K}=(V_{tb}V_{ts}^*\alpha_{em})/(4\pi)$. In the quark sector, the couplings in Eq. (29) also lead to an NP contribution to B_s^0-$\bar{B}_s^0$ mixing at tree level. In Refs. [20, 21], it is assumed that only the LH sector of the quarks has family non-universal $U(1)'$ couplings, as in the current analysis. Thus, only the LH interaction in Eq. (29) contributes to B_s^0-$\bar{B}_s^0$ mixing. They find that one can reproduce the measured value of ΔM_s if

$$\rho_{sb}^L\lesssim 10^{-3}. \quad (51)$$

As a rough estimate, here we take $\rho_{sb}^L=10^{-3}$. Together with Eqs. (38), (39) and

$$V_{tb}=0.999176,\ V_{ts}=-0.03972,\ \alpha_{em}=1/137, \quad (52)$$

we obtain

$$-0.27\lesssim\rho_{ll}^L\lesssim -0.11, \quad (53)$$

$$-0.08\lesssim\rho_{ll}^R\lesssim 0.09. \quad (54)$$

We should emphasize that these parameter ranges are obtained with some assumptions and the current data. In particular, we have used a particular value of ρ_{sb}^L for our illustration. Once new experimental data or theoretical inputs are available, these constraints can easily be updated with our formulas. In Fig. 3 we also give the constraints from Ref. [13]. In their paper, the authors gain the constraints by making the experimental and theoretical values of B → $X_s l^+l^-$ agree with each other in 1σ. However, we get our constraints in 2σ. For a comparison, in Fig. 3 we simply extrapolate their results to 2σ. One can find that if we drop the constraint conditions of flipping the signs of C_9^{eff} and C_{10}, we agree with each other. However, if the A_{FB} is expected to behave as how we get constraints (34) and (35), the constraints in Ref. [13] are too tight to satisfy the conditions.

In Fig. 4 we use the black dot from Fig. 3, where both $C_9^{eff}(q^2)$ and C_{10} flip signs from their SM values, to predict the dA_{FB}/dq^2 spectrum in our model. Since $C_9^{eff}(q^2)$ is q^2-dependent, the plot in Fig. 3 is plotted with C_9 and C_{10} flipping their signs. The points that flip the signs of $C_9^{eff}(q^2)$ and C_{10} should be very close to this point. It is interesting to note that the red dotted curve in Fig. 4 is identical to the usual flipped-sign solution. This is not surprising because flipping the signs of both $C_9^{eff}(q^2)$ and C_{10} simultaneously is equivalent to flipping the sign of C_7^{eff}, which can be seen from Eq. (26). This indicates that by considering only the branching ratios and forward-backward asymmetry of the B → $K^{(*)}l^+l^-$ decays, it is insufficient to determine which operators are significantly modified by the NP.

Now a comment on the form factors is in order. Because of the nonperturbative effects, we cannot get

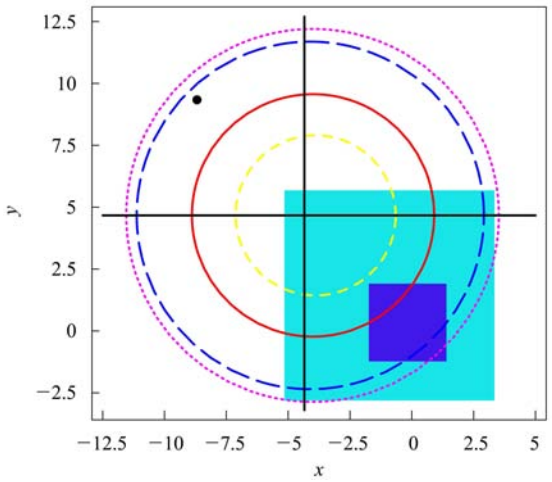

Fig. 3. The constraints from the branching ratios of the $B \to K^{(*)}l^+l^-$ decays. The areas outside the red solid and yellow short dashed circles are determined by Eqs. (45) and (47), respectively. The areas inside the pink and blue circles are determined by Eqs. (46) and (48), respectively. The areas to the left of the line $x = -C_9$ and above the line $y = -C_{10}$ are determined by Eqs. (43) and (44), respectively. The black dot is where both C_9 and C_{10} flip signs from their SM values. The two rectangles, corresponding to S1 (the large rectangle) and S2 (the small rectangle) in Case III, are the constraints given by Ref. [13]. One can see that their constraints are consistent with our constraints from the branching ratios. However, their constraints are not enough to change the signs of C_9 and C_{10}.

good results for the form factors when q^2 is large. In either PQCD or light cone sum rules, the form factors are obtained in a region where q^2 is small and then extrapolated to the entire kinematical region through fitting. As a result, whether the form factors can be described well by the parametrization formula in the large q^2 region is questioned. In fact, the accuracy of the parametrization formula becomes worse as q^2 increases. Therefore, we do not think the theoretical predictions at large q^2 are reliable enough. This may explain why the experimental values are still slightly larger than the theoretical predictions in the large q^2 regime, as shown in Fig. 4.

A closely related decay mode to the current analysis is the $B_s \to \mu^+\mu^-$ decay. This mode has been searched for with great interest at Tevatron. The upper bounds on the branching ratio at 95% confidence

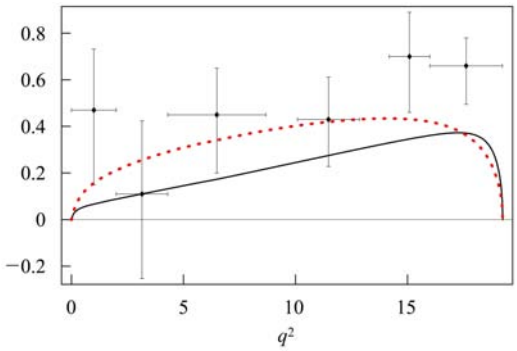

Fig. 4. Forward-backward asymmetry in QCDSR (red dotted line) and PQCD (black solid line) with C_9 and C_{10} flipping their signs (the black dot in Fig. 3). The points with error bars are the experimental results from the Belle Collaboration [7].

level are given by its two experimental groups as

$$\begin{aligned} &Br(B_s \to \mu^+\mu^-) < 5.8\times10^{-8}(\text{CDF}) \quad [22],\\ &Br(B_s \to \mu^+\mu^-) < 1.2\times10^{-7}(\text{D}\emptyset) \quad [23]. \end{aligned} \tag{55}$$

The branching ratio of $B_s \to \mu^+\mu^-$ is affected in our model. With the inclusion of the Z′ contribution, the branching ratio is given by [17]

$$\begin{aligned} &Br(B_s \to \mu^+\mu^-)\\ &= \tau_{B_s}\frac{G_F^2}{4\pi}f_{B_s}^2 m_\mu^2 m_{B_s}\sqrt{1-\frac{4m_\mu^2}{m_{B_s}^2}}\,|V_{tb}^*V_{ts}|^2\\ &\times\left|\frac{\alpha}{2\pi\sin^2\theta_W}Y\left(\frac{m_t^2}{m_W^2}\right)+2\frac{\rho_{bs}^L(\rho_{\mu\mu}^L-\rho_{\mu\mu}^R)}{V_{tb}^*V_{ts}}\right|^2, \end{aligned} \tag{56}$$

where all the functions and symbols are defined in Ref. [17]. With the constraints in Eq. (49), we find that the upper bound for this branching ratio is

$$Br(B_s \to \mu^+\mu^-) \lesssim 7.9\times10^{-9}. \tag{57}$$

Note that the upper bound of the range is still smaller than the current upper bound given by the CDF Collaboration.

4 Summary

We considered the contributions of family nonuniversal Z′ models with flavor-changing neutral currents (Z′ FCNC) at tree level in $B \to K^{(*)}l^+l^-$ decays. By requiring that the theoretically predicted branching ratios agree with the current experimental data

within two σ's, we obtain the constraints on the couplings in the Z′ FCNC model. We find that within the allowed parameter space, our model has the potential to explain the forward-backward asymmetry of the $\mathrm{B}\to\mathrm{K}^*\mathrm{l}^+\mathrm{l}^-$ decay, as better determined by the Belle Collaboration recently. Moreover, our Z′ model contributions flip the signs of $C_9^{\rm eff}$ and C_{10}, which differs from the usual new physics contributions that flip the sign of $C_7^{\rm eff}$. Using the constraints, we also compute the branching ratio of the $\mathrm{B_s}\to\mu^+\mu^-$ decay. The upper bound of our prediction is near the upper bound given by the CDF Collaboration.

C.-W. C. would like to thank the hospitality of IHEP, Beijing, where this project was initiated, during his visit.

Appendix A

Functions for the leptonic and hadronic part

$$L(L,0) = 2\sqrt{q^2}\sin\theta_1, \tag{A1}$$

$$L(L,+) = -2\sqrt{2}\sqrt{q^2}\sin^2\frac{\theta_1}{2}\mathrm{e}^{\mathrm{i}\phi}, \tag{A2}$$

$$L(L,-) = -2\sqrt{2}\sqrt{q^2}\cos^2\frac{\theta_1}{2}\mathrm{e}^{-\mathrm{i}\phi}, \tag{A3}$$

$$L(R,0) = -2\sqrt{q^2}\sin\theta_1, \tag{A4}$$

$$L(R,+) = -2\sqrt{2}\sqrt{q^2}\cos^2\frac{\theta_1}{2}\mathrm{e}^{\mathrm{i}\phi}, \tag{A5}$$

$$L(R,-) = -2\sqrt{2}\sqrt{q^2}\sin^2\frac{\theta_1}{2}\mathrm{e}^{-\mathrm{i}\phi}. \tag{A6}$$

$$\begin{aligned} H(L,0) = {} & \frac{\mathrm{i}G_{\rm F}V_{\rm tb}V_{\rm ts}^*\alpha_{\rm em}}{8\sqrt{2}\pi m_{\mathrm{K}^*}\sqrt{q^2}}\Bigg\{2(C_{7\rm L}-C_{7\rm R})m_{\rm b}\left[\frac{\lambda T_3(q^2)}{m_{\rm B}^2-m_{\mathrm{K}^*}^2}-\left(3m_{\mathrm{K}^*}^2+m_{\rm B}^2-q^2\right)T_2(q^2)\right] \\ & +(C_9^{\rm eff}-C_{10})\left[(m_{\rm B}+m_{\mathrm{K}^*})(m_{\mathrm{K}^*}^2-m_{\rm B}^2+q^2)A_1(q^2)+\frac{\lambda A_2(q^2)}{(m_{\rm B}+m_{\mathrm{K}^*})}\right]\Bigg\}, \end{aligned} \tag{A7}$$

$$\begin{aligned} H(L,+) = {} & \frac{\mathrm{i}G_{\rm F}V_{\rm tb}V_{\rm ts}^*\alpha_{\rm em}}{4\sqrt{2}\pi q^2}\Bigg\{2(C_{7\rm L}+C_{7\rm R})m_{\rm b}\sqrt{\lambda}T_1(q^2)-2(C_{7\rm L}-C_{7\rm R})m_{\rm b}(m_{\rm B}^2-m_{\mathrm{K}^*}^2)T_2(q^2) \\ & +(C_9^{\rm eff}-C_{10})q^2\left[\frac{\sqrt{\lambda}V(q^2)}{(m_{\rm B}+m_{\mathrm{K}^*})}-(m_{\rm B}+m_{\mathrm{K}^*})A_1(q^2)\right]\Bigg\}, \end{aligned} \tag{A8}$$

$$\begin{aligned} H(L,-) = {} & \frac{\mathrm{i}G_{\rm F}V_{\rm tb}V_{\rm ts}^*\alpha_{\rm em}}{4\sqrt{2}\pi q^2}\Bigg\{-2(C_{7\rm L}+C_{7\rm R})m_{\rm b}\sqrt{\lambda}T_1(q^2)-2(C_{7\rm L}-C_{7\rm R})m_{\rm b}(m_{\rm B}^2-m_{\mathrm{K}^*}^2)T_2(q^2) \\ & +(C_9^{\rm eff}-C_{10})q^2\left[-\frac{\sqrt{\lambda}V(q^2)}{(m_{\rm B}+m_{\mathrm{K}^*})}-(m_{\rm B}+m_{\mathrm{K}^*})A_1(q^2)\right]\Bigg\}, \end{aligned} \tag{A9}$$

$$\begin{aligned} H(R,0) = {} & \frac{\mathrm{i}G_{\rm F}V_{\rm tb}V_{\rm ts}^*\alpha_{\rm em}}{8\sqrt{2}\pi m_{\mathrm{K}^*}\sqrt{q^2}}\Bigg\{2(C_{7\rm L}-C_{7\rm R})m_{\rm b}\left[\frac{\lambda T_3(q^2)}{m_{\rm B}^2-m_{\mathrm{K}^*}^2}-\left(3m_{\mathrm{K}^*}^2+m_{\rm B}^2-q^2\right)T_2(q^2)\right] \\ & +(C_9^{\rm eff}+C_{10})\left[(m_{\rm B}+m_{\mathrm{K}^*})(m_{\mathrm{K}^*}^2-m_{\rm B}^2+q^2)A_1(q^2)+\frac{\lambda A_2(q^2)}{(m_{\rm B}+m_{\mathrm{K}^*})}\right]\Bigg\}, \end{aligned} \tag{A10}$$

$$H(R,+) = \frac{\mathrm{i}G_{\mathrm{F}}V_{\mathrm{tb}}V_{\mathrm{ts}}^{*}\alpha_{\mathrm{em}}}{4\sqrt{2}\pi q^2}\Big\{2(C_{7\mathrm{L}}+C_{7\mathrm{R}})m_{\mathrm{b}}\sqrt{\lambda}T_1(q^2)-2(C_{7\mathrm{L}}-C_{7\mathrm{R}})m_{\mathrm{b}}(m_{\mathrm{B}}^2-m_{\mathrm{K}^*}^2)T_2(q^2)$$

$$+(C_9^{\mathrm{eff}}+C_{10})q^2\Big[\frac{\sqrt{\lambda}V(q^2)}{(m_{\mathrm{B}}+m_{\mathrm{K}^*})}-(m_{\mathrm{B}}+m_{\mathrm{K}^*})A_1(q^2)\Big]\Big\}, \tag{A11}$$

$$H(R,-) = \frac{\mathrm{i}G_{\mathrm{F}}V_{\mathrm{tb}}V_{\mathrm{ts}}^{*}\alpha_{\mathrm{em}}}{4\sqrt{2}\pi q^2}\Big\{-2(C_{7\mathrm{L}}+C_{7\mathrm{R}})m_{\mathrm{b}}\sqrt{\lambda}T_1(q^2)-2(C_{7\mathrm{L}}-C_{7\mathrm{R}})m_{\mathrm{b}}(m_{\mathrm{B}}^2-m_{\mathrm{K}^*}^2)T_2(q^2)$$

$$+(C_9^{\mathrm{eff}}+C_{10})q^2\Big[-\frac{\sqrt{\lambda}V(q^2)}{(m_{\mathrm{B}}+m_{\mathrm{K}^*})}-(m_{\mathrm{B}}+m_{\mathrm{K}^*})A_1\left(q^2\right)\Big]\Big\}. \tag{A12}$$

References

1 Jaus W, Wyler D. Phys. Rev. D, 1990, **41**: 3405; Colangelo P, De Fazio F, Santorelli P, Scrimieri E. Phys. Rev. D, 1996, **53**: 3672; 1998, **57**: 3186 [arXiv:hep-ph/9510403]; Aliev T M, Ozpineci A, Savci M. Phys. Rev. D, 1997, **56**: 4260 [arXiv:hep-ph/9612480]; Melikhov D, Nikitin N, Simula S. Phys. Lett. B, 1998, **430**: 332 [arXiv:hep-ph/9803343]

2 Burdman G. Phys. Rev. D, 1995, **52**: 6400 [arXiv:hep-ph/9505352]; Burdman G. Phys. Rev. D, 1998, **57**: 4254 [arXiv:hep-ph/9710550]; Beneke M, Feldmann T, Seidel D. Nucl. Phys. B, 2001, **612**: 25 [arXiv:hep-ph/0106067]; Feldmann T, Matias J. JHEP 2003, **0301**: 074 [arXiv:hep-ph/0212158]; Kruger F, Matias J. Phys. Rev. D, 2005, **71**: 094009 [arXiv:hep-ph/0502060]

3 Hewett J L, Wells J D. Phys. Rev. D, 1997, **55**: 5549 [arXiv:hep-ph/9610323]; Ali A, Ball P, Handoko L T, Hiller G. Phys. Rev. D, 2000, **61**: 074024 [arXiv:hep-ph/9910221]; Colangelo P, De Fazio F, Ferrandes R, Pham T N. Phys. Rev. D, 2006, **73**: 115006 [arXiv:hep-ph/0604029]; Hovhannisyan A, HOU W S, Mahajan N. Phys. Rev. D, 2008, **77**: 014016 [arXiv:hep-ph/0701046]

4 Ishikawa A et al. Phys. Rev. Lett., 2006, **96**: 251801 [arXiv:hep-ex/0603018]

5 Aubert B et al. (BABAR collaboration). Phys. Rev. Lett., 2009, **102**: 091803 [arXiv:0807.4119 [hep-ex]]

6 Aubert B et al. (BABAR collaboration). Phys. Rev. D, 2009, **79**: 031102 [arXiv:0804.4412 [hep-ex]]

7 WEI J T et al. (BELLE collaboration). Phys. Rev. Lett., 2009, **103**: 171801 [arXiv:0904.0770 [hep-ex]]

8 Langacker P, Plumacher M. Phys. Rev. D, 2000, **62**: 013006 [arXiv:hep-ph/0001204]

9 Barger V, Chiang C W, Langacker P, Lee H S. Phys. Lett. B, 2004, **580**: 186 [arXiv:hep-ph/0310073]; Barger V, Chiang C W, JIANG J, Langacker P. Phys. Lett. B, 2004 **596**; 229 [arXiv:hep-ph/0405108]; Barger V, Chiang C W, Langacker P, Lee H S. Phys. Lett. B, 2004, **598**: 218 [arXiv:hep-ph/0406126]; Arhrib A, Cheung K, Chiang C W, YUAN T C. Phys. Rev. D, 2006, **73**: 075015 [arXiv:hep-ph/0602175]; Cheung K, Chiang C W, Deshpande N G, JIANG J. Phys. Lett. B, 2007, **652**: 285 [arXiv:hep-ph/0604223]; Chiang C W, Deshpande N G, JIANG J. JHEP, 2006, **0608**: 075 [arXiv:hep-ph/0606122]

10 HE X G, Valencia G. Phys. Rev. D, 2004, **70**: 053003 [arXiv:hep-ph/0404229]; Phys. Lett. B, 2007, **651**: 135 [arXiv:hep-ph/0703270]

11 Barger V, Everett L, JIANG J, Langacker P, LIU T, Wagner C. Phys. Rev. D, 2009, **80**: 055008 [arXiv:0902.4507 [hep-ph]]; arXiv:0906.3745 [hep-ph]

12 CHEN S L, Okada N. Phys. Lett. B, 2008, **669**: 34 [arXiv:0808.0331 [hep-ph]]

13 CHANG Q, LI X Q, YANG Y D. JHEP 2009, **0905**: 056 [arXiv:0903.0275 [hep-ph]]; arXiv:0907.4408 [hep-ph]

14 Keum Y Y, LI H N, Sanda A I. Phys. Lett. B, 2001, **504**: 6 [arXiv:hep-ph/0004004]; LÜ C D, Ukai K, YANG M Z. Phys. Rev. D, 2001, **63**: 074009 e-Print: hep-ph/0004213; Keum Y, LI H N. Phys. Rev. D, 2001, **63**: 074006 [arXiv:hep-ph/0006001]; LÜ C D, YANG M Z. Eur. Phys. J. C, 2002, **23**: 275–287 e-Print: hep-ph/0011238

15 Ball P, Braun V M. Phys. Rev. D, 1998, **58**: 094016 [arXiv:hep-ph/9805422]

16 Ali A, Ball P, Handoko L T, Hiller G. Phys. Rev. D, 2000, **61**: 074024

17 Buchalla G, Buras A J, Lautenbacher M E. Rev. Mod. Phys., 1996, **68**: 1125 [arXiv:hep-ph/9512380]

18 Buras A J, Munz M. Phys. Rev. D, 1995, **52**: 186 [arXiv:hep-ph/9501281]

19 LI R H , LÜ C D, WANG W. Phys. Rev. D, 2009, **79**: 094024 [arXiv:0902.3291 [hep-ph]]

20 Cheung K, Chiang C W, Deshpande N G, JIANG J. Phys. Lett. B, 2007, **652**: 285

21 Barger V, Everett L, JIANG J, Langacker P, LIU T, Wagner C. Phys. Rev. D, 2009, **80**: 055008[arXiv:0902.4507 [hep-ph]]; arXiv:0906.3745[hep-ph]; Barger V, Everett L L, JIANG J, Langacker P, LIU T, Wagner C E M. JHEP, 2009, **0912**: 048[arXiv:0906.3745 [hep-ph]]

22 Aaltonen T et al. (CDF collaboration). Phys. Rev. Lett., 2008, **100**: 101802 [arXiv:0712.1708 [hep-ex]]

23 Abazov V M et al. (D0 collaboration). Phys. Rev. D, 2007, **76**: 092001 [arXiv:0707.3997 [hep-ex]]